pathoexcitation via an increase in oxidative stress. *Circ Res* 96: 252–260, 2005.

55. **Kimura Y, Hirooka Y, Sagara Y, Sunagawa K.** Long-acting calcium channel blocker, azelnidipine, increases endothelial nitric oxide synthase in the brain and inhibits sympathetic nerve activity. *Clin Exp Hypertens* 29: 13–21, 2007.
56. **Kimura Y, Hirooka Y, Kishi T, Ito K, Sagara Y, Sunagawa K.** Role of inducible nitric oxide synthase in rostral ventrolateral medulla in blood pressure regulation in spontaneously hypertensive rats. *Clin Exp Hypertens* 31: 281–286, 2009.
57. **Kishi T, Hirooka Y, Shigematsu H, Shimokawa H, Takeshita A.** Overexpression of eNOS in the RVLM causes hypotension and bradycardia via GABA release. *Hypertension* 38: 896–901, 2001.
58. **Kishi T, Hirooka Y, Ito K, Sakai K, Shimokawa H, Takeshita A.** Cardiovascular effects of overexpression of endothelial nitric oxide synthase in the rostral ventrolateral medulla in stroke-prone spontaneously hypertensive rats. *Hypertension* 39: 264–268, 2002.
59. **Kishi T, Hirooka Y, Mukai Y, Shimokawa H, Takeshita A.** Atorvastatin causes depressor and sympatho-inhibitory effect with upregulation of nitric oxide synthases in stroke-prone hypertensive rats. *J Hypertens* 21: 379–386, 2003.
60. **Kishi T, Hirooka Y, Kimura Y, Sakai K, Ito K, Shimokawa H, Takeshita A.** Overexpression of eNOS in RVLM improves impaired baroreflex control of heart rate in SHRSP. *Hypertension* 41: 255–260, 2003.
61. **Kishi T, Hirooka Y, Kimura Y, Ito K, Shimokawa H, Takeshita A.** Increased reactive oxygen species in rostral ventrolateral medulla contribute to neural mechanisms of hypertension in stroke-prone spontaneously hypertensive rats. *Circulation* 109: 2357–2362, 2004.
62. **Kishi T, Hirooka Y, Shimokawa H, Takeshita A, Sunagawa K.** Atorvastatin reduces oxidative stress in the rostral ventrolateral medulla of stroke-prone spontaneously hypertensive rats. *Clin Exp Hypertens* 30: 3–11, 2008.
63. **Kishi T, Hirooka Y, Konno S, Sunagawa K.** Atorvastatin improves the impaired baroreflex sensitivity via anti-oxidant effect in the rostral ventrolateral medulla of SHRSP. *Clin Exp Hypertens* 31: 698–704, 2009.
64. **Kishi T, Hirooka Y, Konno S, Sunagawa K.** Sympathoinhibition induced by centrally administered atorvastatin is associated with alteration of NAD(P)H and Mn-SOD activity in rostral ventrolateral medulla of stroke-prone SHR. *J Cardiovasc Pharmacol* 55: 184–190, 2010.
65. **Kishi T, Hirooka Y, Konno S, Ogawa K, Sunagawa K.** Angiotensin type 1 receptor-activated caspase-3 through ras/mitogen-activated protein kinase/extracellular signal-regulated kinase in the rostral ventrolateral medulla is involved in sympathoexcitation in stroke-prone spontaneously hypertensive rats. *Hypertension* 55: 291–297, 2010.
66. **Koga Y, Hirooka Y, Araki S, Nozoe M, Kishi T, Sunagawa K.** High salt intake enhances blood pressure increase during development of hypertension via oxidative stress in rostral ventrolateral medulla of spontaneously hypertensive rats. *Hypertens Res* 31: 2075–2083, 2008.
67. **Konno S, Hirooka Y, Araki S, Koga Y, Kishi T, Sunagawa K.** Azelnidipine decreases sympathetic nerve activity via antioxidant effect in the rostral ventrolateral medulla of stoke-prone spontaneously hypertensive rats. *J Cardiovasc Pharmacol* 52: 555–560, 2008.
68. **Kung LC, Chan SHH, Wu KLH, Ou CC, Tai MH, Chan JYH.** Mitochondrial respiratory enzyme complexes in rostral ventrolateral medulla as cellular targets of nitric oxide and superoxide interaction in the antagonism of antihypertensive action of eNOS transgene. *Mol Pharmacol* 74: 1319–1332, 2008.
69. **Kurukoff TL, Gehlen F, Ganten D, Wagner J.** Gene expression of brain nitric oxide synthase and soluble guanylate cyclase in hypothalamus and medulla of two-kidney, one-clip hypertensive rats. *Hypertension* 26: 171–176, 1995.
70. **Krukoff TL.** Central action of nitric oxide in regulation of autonomic functions. *Brain Res Rev* 30: 52–65, 1999.
71. **Lambeth JD.** Nox enzymes, ROS, and chronic disease: an example of antagonistic pleiotropy. *Free Radic Biol Med* 43: 332–347, 2007.
72. **Lassegue B, Clempus RE.** Vascular NAD(P)H oxidases: specific features, expression, and regulation. *Am J Physiol Regul Integr Comp Physiol* 285: R277–R297, 2003.
73. **Leenen FHH, Ruzicka M, Huang BS.** Central sympathoinhibitory effects of calcium channel blockers. *Curr Hypertens Res* 3: 314–321, 2001.
74. **Lin HC, Kang BH, Wan FJ, Huang ST, Tseng CJ.** Reciprocal regulation of nitric oxide and glutamate in the nucleus tractus solitarii of rats. *Eur J Pharmacol* 407: 83–89, 2000.
75. **Lin LH.** Glutamatergic neurons say NO in the nucleus tractus solitarii. *J Chem Neuroanat* 38: 1154–165, 2009.
76. **Lin Y, Matsumura K, Kagiyama S, Fukuhara M, Fujii K, Iida M.** Chronic administration of olmesartan attenuates the exaggerated pressor response to glutamate in the rostral ventrolateral medulla of SHR. *Brain Res* 1058: 161–166, 2005.
77. **Liu D, Gao L, Roy SK, Cornish KG, Zucker IH.** Neuronal angiotensin II type 1 receptor upregulation in heart failure: activation of activator protein 1 and jun N-terminal kinase. *Circ Res* 99: 1004–1011, 2006.
78. **Liu JL, Murakami H, Zucker IH.** Effects of NO on baroreflex control of heart rate and renal nerve activity in conscious rabbits. *Am J Physiol Regul Integr Comp Physiol* 270: R1361–R1370, 1996.
79. **Luft FC, Demmert G, Rohmeiss P, Unger T.** Baroreceptor reflex effect on sympathetic nerve activity in stroke-prone spontaneously hypertensive rats. *J Auton Nerv Syst* 17: 199–209, 1986.
80. **Ma S, Abboud FM, Felder RB.** Effects of L-arginine-derived nitric oxide synthesis on neuronal activity in nucleus tractus solitarius. *Am J Physiol Regul Integr Comp Physiol* 268: R487–R491, 1995.
81. **Marting-Pinge MC, Baraldi-Passy I, Lopes OU.** Excitatory effects of nitric oxide within the rostral ventrolateral medulla of freely moving rats. *Hypertension* 30: 704–707, 1997.
82. **Matsuo I, Hirooka Y, Hironaga K, Eshima K, Shigematsu H, Shihara M, Sakai K, Takeshita A.** Glutamate release via NO production evoked by NMDA in the NTS enhances hypotension and bradycardia in vivo. *Am J Physiol Regul Integr Comp Physiol* 280: R1285–R1291, 2001.
83. **McKinley MJ, Albinson AL, Allen AM, Mathai M, May CN, McAllen RM, Oldfield BJ, Mendelsohn FAO, Chai SY.** The brain renin-angiotensin system: location and physiological roles. *Int J Biochem Cell Biol* 35: 901–918, 2003.
84. **Mogi M, Horiuchi M.** Remote control of brain angiotensin II levels by angiotensin receptor blockers. *Hypertens Res* 33: 116–117, 2010.
85. **Morimoto S, Cassel MD, Beltz TG, Johnson AK, Davisson RL, Sigmund CD.** Elevated blood pressure in transgenic mice with brain-specific expression of human angiotensinogen driven by the glial fibrillary acidic protein promoter. *Circ Res* 89: 365–372, 2001.
86. **Morimoto S, Cassell MD, Sigmund CD.** The brain renin-angiotensin system in transgenic mice carrying a highly regulated human renin transgene. *Circ Res* 90: 80–86, 2002.
87. **Murakami H, Liu JL, Yoneyama H, Nishida Y, Okada K, Kosaka H, Morita H, Zucker IH.** Blockade of neuronal nitric oxide synthase alters the baroreflex control of heart rate in the rabbit. *Am J Physiol Regul Integr Comp Physiol* 274: R181–R186, 1998.
88. **Murphy S, Gibson CL.** Nitric oxide, ischaemia and brain inflammation. *Biochem Soc Trans* 35: 1133–1137, 2007.
89. **Nishimura Y, Ito T, Hoe KL, Saavedra JM.** Chronic peripheral administration of the angiotensin II AT_1 receptor antagonist candesartan blocks brain AT_1 receptors. *Brain Res* 871: 29–38, 2000.
90. **Nozoe M, Hirooka Y, Koga Y, Sagara Y, Kishi T, Engelhardt JF, Sunagawa K.** Inhibition of rac1-derived reactive oxygen species in nucleus tractus solitarius decreases blood pressure and heart rate in stroke-prone spontaneously hypertensive rats. *Hypertension* 50: 62–68, 2007.
91. **Nozoe M, Hirooka Y, Koga Y, Araki S, Konno S, Kishi T, Ide T, Sunagawa K.** Mitochondria-derived reactive oxygen species mediate sympathoexcitation induced by angiotensin II in the rostral ventrolateral medulla. *J Hypertens* 26: 2176–2184, 2008.
92. **Oliveira-Sales EB, Dugaich AP, Carillo BA, Abreu NP, Boim MA, Martins PJ, D'Almeida V, Dolnkoff MS, Bergamaschi CT, Campos RR.** Oxidative stress contributes to renovascular hypertension. *Am J Hypertens* 21: 98–104, 2008.
93. **Oliveira-Sales EB, Nishi EE, Carillo BA, Dolnikoff MS, Bergamaschi CT, Campos RR.** Oxidative stress in the sympathetic premotor neurons contributes to sympathetic activation in renovascular hypertension. *Am J Hypertens* 22: 484–492, 2009.
94. **Paravicini T, Touyz RM.** Redox signaling in hypertension. *Cardiovasc Res* 71: 247–258, 2006.
95. **Patel KP, Li YF, Hirooka Y.** Role of nitric oxide in central sympathetic outflow. *Exp Biol Med (Maywood)* 226: 814–824, 2001.

96. **Paton JFR, Waki H, Abdala APL, Dickinson J, Kasparov S.** Vascular-brain signaling in hypertension: role of angiotensin II and nitric oxide. *Curr Hypertens Rep* 9: 242–247, 2007.
97. **Pannu R, Singh I.** Pharmacological strategies for the regulation of inducible nitric oxide synthase: neurogenerative versus neuroprotective mechanisms. *Neurochem Intl* 49: 170–182, 2006.
98. **Pelisch N, Hosomi N, Ueno M, Masugata H, Murao K, Hitomi H, Nakao D, Kobori H, Nishiyama A, Kohno M.** Systemic candesartan reduces brain angiotensin II via downregulation of brain renin-angiotensin system. *Hypertens Res* 33: 161–164, 2010.
99. **Peterson JR, Shrama RV, Davisson RL.** Reactive oxygen species in the neuropathogenesis of hypertension. *Curr Hypertens Rep* 8: 232–241, 2006.
100. **Pilowsky P, Goodchild AK.** Baroreceptor reflex pathways and neurotransmitters: 10 years on. *J Hypertens* 20: 1675–1688, 2002.
101. **Plochocka-Zulinska D, Krukoff TL.** Increased gene expression of neuronal nitric oxide synthase in brain of adult spontaneously hypertensive rats. *Mol Brain Res* 48: 291–297, 1997.
102. **Polizio AH, Peña C.** Effects of angiotensin II type 1 receptor blockade on the oxidative stress in spontaneously hypertensive rat tissues. *Regul Pept* 128: 1–5, 2005.
103. **Pontieri V, Venezuela MK, Scavone C, Michelini LC.** Role of endogenous nitric oxide in the nucleus tractus solitarii on baroreflex control of heart rate in spontaneously hypertensive rats. *J Hypertens* 16: 1993–1999, 1998.
104. **Qadri F, Arens T, Schwarz EC, Häuser W, Dendorfer A, Dominiak P.** Brain nitric oxide synthase activity in spontaneously hypertensive rats during development of hypertension. *J Hypertens* 21: 1687–1694, 2003.
105. **Reja V, Goodchild AK, Phillips JK, Pilowski PM.** Upregulation of angiotensin AT_1 receptor and intracellular kinase gene expression in hypertensive rats. *Clin Exp Pharmacol Physiol* 33: 690–695, 2006.
106. **Ren J.** Influence of gender on oxidative stress, lipid peroxidation, protein damage and apoptosis in hearts and brains from spontaneously hypertensive rats. *Clin Exp Pharmacol Physiol* 34: 432–438, 2007.
107. **Sakai K, Hirooka Y, Matsuo I, Eshima K, Shigematsu H, Shimokawa H, Takeshita A.** Overexpression of eNOS in NTS causes hypotension and bradycardia in vivo. *Hypertension* 36: 1023–1028, 2000.
108. **Sakai K, Agassandian K, Morimoto S, Sinnayah P, Cassell MD, Davisson RL, Sigmund CD.** Local production of angiotensin II in the subfornical organ causes elevated drinking. *J Clin Invest* 117: 1088–1095, 2007.
109. **Sander M, Chavoshan B, Victor RG.** A large blood pressure-raising effect of nitric oxide synthase inhibition in humans. *Hypertension* 33: 937–942, 1999.
110. **Sano H, Matsumoto K, Utsumi H.** Synthesis and imaging of blood-brain-barrier permeable nitroxyl-probes for free radicals reactions in brain of living mice. *Biochem Mol Biol Int* 42: 641–647, 1997.
111. **Sano H, Naruse M, Matsumoto K, Oi T, Utsumi H.** A new nitroxy-probe with high retention in the brain and its application for brain imaging. *Free Radic Biol Med* 28: 959–969, 2000.
112. **Shapoval LN, Sagach VF, Pobegailo LS.** Nitric oxide influences ventrolateral medullary mechanisms of vasomotor control in the cat. *Neurosci Lett* 132: 47–50, 1991.
113. **Sun C, Sellers KW, Sumners C, Raizada MK.** NAD(P)H oxidase inhibition attenuates neuronal chronotropic actions of angiotensin II. *Circ Res* 96: 659–666, 2005.
114. **Sun J, Druhan LJ, Zweier JL.** Reactive oxygen and nitrogen species regulate inducible nitric oxide synthase function shifting the balance of nitric oxide and superoxide production. *Arch Biochem Biophys* 494: 130–137, 2010.
115. **Sved AF, Ito S, Sved JC.** Brainstem mechanisms of hypertension: role of the rostral ventrolateral medulla. *Curr Hypertens Rep* 5: 262–268, 2003.
116. **Tagawa T, Imaizumi T, Harada S, Endo T, Shiramoto M, Hirooka Y, Takeshita A.** Nitric oxide influences neuronal activity in the nucleus tractus solitarius of rat brainstem slices. *Circ Res* 75: 70–76, 1994.
117. **Tai MH, Wang LL, Wu KLH, Chan JYH.** Increased superoxide anion in rostral ventrolateral medulla contributes to hypertension in spontaneously hypertensive rats via interactions with nitric oxide. *Free Radic Biol Med* 38: 450–462, 2005.
118. **Talman WT, Dragon DN.** Transmission of arterial baroreflex signals depends on neuronal nitric oxide synthase. *Hypertension* 43: 820–824, 2004.
119. **Talman WT.** NO and central cardiovascular control: a simple molecule with a complex story. *Hypertension* 48: 552–554, 2006.
120. **Tseng CJ, Liu HY, Lin HC, Ger LP, Tung CS, Yen MH.** Cardiovascular effects of nitric oxide in the brain stem nuclei of rats. *Hypertension* 27: 36–42, 1996.
121. **Waki H, Murphy D, Yao ST, Kasparov S, Paton JFR.** Endothelial NO synthase activity in nucleus tractus solitarii contributes to hypertension in spontaneously hypertensive rats. *Hypertension* 48: 644–650, 2006.
122. **Wang G, Anrather J, Huang J, Speth RC, Pickel VM, Iadecola C.** NADPH oxidase contributes angiotensin signaling in the nucleus tractus solitarius. *J Neurosci* 24: 5516–5524, 2004.
123. **Wang G, Anrather J, Glass MJ, Tarsitano J, Zhou P, Frys KA, Pickel VM, Iadecola C.** Nox2, Ca^{2+}, and protein kinase C play a role in angiotensin II-induced free radical production in nucleus tractus solitarius. *Hypertension* 48: 482–489, 2006.
124. **Wang JM, Tan J, Leenen FHH.** Central nervous system blockade by peripheral administration of AT_1 receptor blockers. *J Cardiovasc Pharmacol* 41: 593–599, 2003.
125. **Wang S, Paton JFR, Kasparov.** Differential sensitivity of excitatory and inhibitory synaptic transmission to modulation by nitric oxide in rat nucleus tractus solitarii. *Exp Physiol* 92: 371–382, 2007.
126. **Wu SY, Dun NJ.** Potentiation of IPSCs by nitric oxide in immature rat sympathetic preganglionic neurons in vitro. *J Physiol* 495: 479–490, 1996.
127. **Wu SY, Dun NJ.** Nitric oxide and excitatory postsynaptic currents in immature rat sympathetic preganglionic neurons in vitro. *Neuroscience* 79: 237–245, 1997.
128. **Yin JX, Yang RF, Li S, Renshaw AO, Li YL, Schultz HD, Zimmerman MC.** Mitochondria-produced superoxide mediates angiotensin II-induced inhibition of neuronal potassium current. *Am J Physiol Cell Physiol* 298: C857–C865, 2010.
129. **Zanzinger J.** Role of nitric oxide in the neural control of cardiovascular function. *Cardiovasc Res* 43: 639–649, 1999.
130. **Zanzinger J.** Mechanisms of action of nitric oxide in the brain stem: role of oxidative stress. *Auton Neurosci* 98: 24–27, 2002.
131. **Zanzinger J, Czachurski J, Seller H.** Inhibition of basal and reflex-mediated sympathetic activity in the RVLM by nitric oxide. *Am J Physiol Regul Integr Comp Physiol* 268: R958–R962, 1995.
132. **Zimmerman MC, Lazartigues E, Lang JA, Sinnayah P, Ahmad IM, Spitz DR, Davisson RL.** Superoxide mediates the actions of angiotensin II in the central nervous system. *Circ Res* 91: 1038–1045, 2002.
133. **Zimmerman MC, Lazartigues E, Sharma RV, Davisson RL.** Hypertension caused by angiotensin II infusion involves increased superoxide production in the central nervous system. *Circ Res* 95: 210–216, 2004.
134. **Zimmerman MC, Dunlay RP, Larzartigues E, Zhang Y, Sharma RV, Engelhardt JF, Davisson RL.** Requirement for Rac-1dependent NADPH oxidase in the cardiovascular and dipsogenic actions of angiotensin II in the brain. *Circ Res* 95: 532–539, 2004.
135. **Zimmerman MC, Sharma RV, Davisson RL.** Superoxide mediates angiotensin II-induced influx of extracellular calcium in neural cells. *Hypertension* 45: 717–723, 2005.
136. **Zimmerman MC, Zucker IH.** Mitochondrial dysfunction and mitochondrial-produced reactive oxygen species: new targets for neurogenic hypertension? *Hypertension* 53: 112–114, 2009.

Nanoparticle-Mediated Delivery of Pitavastatin Into Lungs Ameliorates the Development and Induces Regression of Monocrotaline-Induced Pulmonary Artery Hypertension

Ling Chen, Kaku Nakano, Satoshi Kimura, Tetsuya Matoba, Eiko Iwata, Miho Miyagawa, Hiroyuki Tsujimoto, Kazuhiro Nagaoka, Junji Kishimoto, Kenji Sunagawa, Kensuke Egashira

Abstract—Pulmonary artery hypertension (PAH) is an intractable disease of the small PAs in which multiple pathogenic factors are involved. Statins are known to mitigate endothelial injury and inhibit vascular remodeling and inflammation, all of which play crucial roles in the pathogenesis of PAH. We tested the hypothesis that nanoparticle (NP)-mediated delivery of pitavastatin into the lungs can be a novel therapeutic approach for the treatment of PAH. Among the marketed statins, pitavastatin was found to have the most potent effects on proliferation of PA smooth muscle cells in vitro. We formulated pitavastatin-NP and found that pitavastatin-NP was more effective than pitavastatin alone in inhibiting cellular proliferation and inflammation in vitro. In a rat model of monocrotaline-induced PAH, a single intratracheal instillation of NP resulted in the delivery of NP into alveolar macrophages and small PAs for up to 14 days after instillation. Intratracheal treatment with pitavastatin-NP, but not with pitavastatin, attenuated the development of PAH and was associated with a reduction of inflammation and PA remodeling. NP-mediated pitavastatin delivery was more effective than systemic administration of pitavastatin in attenuating the development of PAH. Importantly, treatment with pitavastatin-NP 3 weeks after monocrotaline injection induced regression of PAH and improved survival rate. This mode of NP-mediated pitavastatin delivery into the lungs is effective in attenuating the development of PAH and inducing regression of established PAH, suggesting potential clinical significance for developing a new treatment for PAH. (***Hypertension.*** **2011;57:343-350.)** • **Online Data Supplement**

Key Words: pulmonary hypertension ■ nanotechnology ■ pitavastatin ■ inflammation ■ leukocytes

Pulmonary artery hypertension (PAH) is an intractable disease of the small PAs resulting in progressive increases in pulmonary vascular resistance, right ventricular (RV) failure, and ultimately premature death.[1,2] Mortality from PAH remains high, even after introduction of vasodilator therapies such as prostacyclin infusion, endothelin receptor antagonists, and phosphodiesterase inhibitors (which have raised the 5-year survival rate to ≈50%). Although these drugs were originally developed for non-PAH vascular diseases, they were introduced into treatment for clinical PAH on the basis of the vasodilator hypothesis. Therefore, a new idea that might lead to a breakthrough curative treatment for PAH is urgently needed.

In addition to vasoconstriction, other multiple factors (endothelial injury/apoptosis, obstructive vascular remodeling, proliferation, and inflammation) play an important role in the mechanism of PAH.[1,2] Therefore, we hypothesized that a controlled, local delivery system targeting a battery of those pathogenic factors intrinsic to PAH pathology would be a favorable therapeutic approach with high translational potential to clinical medicine. In this respect, we focused on the vasculoprotective effects of 3-hydroxy-3-methylglutaryl coenzyme A reductase inhibitors, the so-called statins. Statins are known to increase expression and activity of endothelial nitric oxide synthase (eNOS) and thus ameliorate endothelial injury.[3–6] Prior studies have reported that systemic administration of statins attenuates monocrotaline (MCT)-induced and hypoxia-induced PAH in animals.[7–9] These beneficial therapeutic effects of statins on PAH, however, were observed after daily administration of high doses of statins, a regimen that could lead to serious adverse side effects in the clinical setting. However, not all studies have reported beneficial effects of statins with regard to PAH in animal models.[10,11] We recently reported that (1) intratracheal administration of bioabsorbable polymeric nanoparticles (NPs) represented a novel drug delivery system into the lung; and (2) NP-mediated delivery of a nuclear factor (NF)-κB decoy into the lungs effectively inhibited NF-κB–mediated inflammation and thus, attenuated the development and progression of PAH in a rat model of MCT-induced PAH.[12] This

Received May 23, 2010; first decision June 21, 2010; revision accepted December 8, 2010.

From the Department of Cardiovascular Medicine (L.C., K.N., T.M., E.I., M.M., K.N., K.S., K.E.) and Digital Medicine Initiative (J.K.), Graduate School of Medical Science, Kyushu University, Fukuoka, and Hosokawa Micron Corporation (H.T.), Osaka, Japan.

Correspondence to Kensuke Egashira, Department of Cardiovascular Medicine, Graduate School of Medical Science, Kyushu University, 3-1-1, Maidashi, Higashi-ku, Fukuoka 812-8582, Japan. E-mail egashira@cardiol.med.kyushu-u.ac.jp

Hypertension **is available at http://hyper.ahajournals.org** **DOI: 10.1161/HYPERTENSIONAHA.110.157032**

nanotechnology platform may optimize the efficacy and minimize the potential side effects of drugs.

Therefore, the primary aim of this study was to test the hypothesis that NP-mediated local delivery of statins to the lung is an innovative therapeutic approach for PAH. Pitavastatin was selected as the nanoparticulation compound because this drug has shown the most potent beneficial effects on human endothelial and smooth muscle cells in vitro compared with other statins.[13,14] We then used a rat model of MCT-induced PAH and examined (1) whether this NP-mediated delivery of pitavastatin into the lung is more effective than intratracheal or systemic administration of pitavastatin in attenuating the development of PAH and (2) whether this NP-mediated delivery system induces regression of established PAH.

Materials and Methods

Human PA Smooth Muscle Cell Proliferation Assay

Human PA smooth muscle cells (PASMCs) were seeded on 96-well culture plates at 10^4 cells per well in SmBM. After 24 hours of starvation, 10% fetal bovine serum was added for cell stimulation. In addition, various concentrations of statins (simvastatin, pitavastatin, atorvastatin, losuvastatin, fluvastatin, and pravastatin) or vehicle were added (n=6 per group). Statins were purchased, extracted from products, and purified. Cells were incubated for another 24 hours after addition of 5′-bromo-2′-deoxyuridine, and 5′-bromo-2′-deoxyuridine incorporation was evaluated by an ELISA kit from Calbiochem.

In another set of experiments, a 1.0-mL suspension of pitavastatin at 5 mg/mL, fluorescein isothiocyanate (FITC)–NP (1 mg/mL lactide/glycolide copolymer [PLGA]), pitavastatin-NP containing 1.0 mg/mL PLGA and 5 mg/mL pitavastatin, or vehicle was added to each well (n=6 per group). Cells were incubated for another 4 days, and the cells were fixed with methanol and stained with Diff-Quick staining solution. A single observer counted the number of cells per plate.

Preparation of PLGA-NP

A PLGA with an average molecular weight of 20 000 and a copolymer ratio of lactide to glycolide of 75:25 (Wako Pure Chemical Industries, Osaka, Japan) was used as wall material for the NP. PLGA-NP incorporated with FITC or pitavastatin (Kowa Pharmaceutical Co Ltd, Tokyo, Japan) was prepared by a previously reported emulsion solvent diffusion method in purified water.[15,16] PLGA was dissolved in a mixture of acetone and methanol. Then, FITC or pitavastatin was added to this solution. The resultant PLGA-FITC or PLGA-statin solution was emulsified in a polyvinyl alcohol solution with stirring at 400 rpm by using a propeller-type agitator with 3 blades (Heidon 600G, Shinto Scientific, Tokyo, Japan). After the system was agitated for 2 hours under reduced pressure at 40°C, the entire suspension was centrifuged (20 000*g* for 20 minutes at −20°C). After the supernatant was removed, purified water was added and mixed with the sediment. The wet mixture was then centrifuged again to remove the excess polyvinyl alcohol and the unencapsulated reagent that could not adsorb onto the surfaces of the NPs. After this process was repeated, the resultant dispersion was freeze-dried under the same conditions. The FITC- and pitavastatin-loaded PLGA-NP contained 13% (wt/vol) FITC and 13% (wt/vol) pitavastatin, respectively. A sample of NP suspension in distilled water was used for particle size analysis. The diameter of NPs was 196±29 nm. Surface charge (zeta potential) was also analyzed by Zetasizer Nano (Sysmex, Hyogo, Japan) and was anionic (−15±10 mV at pH 4.4).

Experimental Animal Models

All experiments were reviewed and approved by the committee on ethics on animal experiments, Kyushu University Faculty of Medicine, and were conducted according to the guidelines of the American Physiological Society. Adult male Sprague-Dawley rats (Charles River, Yokohama, Japan; 250 to 300 g body weight) were injected subcutaneously with 60 mg/kg MCT (Wako), which induces severe PAH in 3 weeks.[12,17]

In a prevention protocol, animals were divided into 4 groups that received intratracheal instillation of phosphate-buffered saline (PBS), pitavastatin only (100 μg), FITC-NP (1 mg PLGA), or pitavastatin-NP (100 μg pitavastatin per mg PLGA) immediately after MCT injection. For intratracheal instillation, a 0.1-mL suspension of pitavastatin, FITC-NP, or pitavastatin-NP was injected gently into the trachea of animals, accompanied by an equal volume of air. This dose of pitavastatin was selected because we examined the effects of intratracheal instillation of various concentrations and volumes of pitavastatin suspension (10, 30, 100, or 300 μg per animal in 0.05, 0.1, and 0.2 mL PBS) and confirmed that a 0.1-mL suspension of pitavastatin containing 100 μg pitavastatin was an optimal dose in our experiments. In a treatment protocol, rats were divided into 4 groups that received intratracheal instillation of PBS, pitavastatin only (100 μg), FITC-NP (1 mg PLGA), or pitavastatin-NP (100 μg pitavastatin per mg PLGA) 21 days after MCT injection when severe PAH had already been established. In another set of experiments, 3 other groups received systemic daily oral pitavastatin at doses of 0.3, 1.0, 3.0, and 10 mg/kg, dissolved in 0.5% carboxymethyl cellulose, by gavage from the day of MCT injection until the mice were euthanized on day 21.

Biodistribution of FITC-NP After Intratracheal Administration Into the Lung

Biodistribution of FITC in the lung was examined in rats that received intratracheal instillation of FITC-NP. Animals were euthanized and the tracheas were exposed. The lungs were inflated with a solution of 10% phosphate-buffered formalin (pH 7.4) by using a catheter inserted into the trachea. The lungs were then removed en bloc and placed into 10% phosphate-buffered formalin for a further 12 to 18 hours. After light and fluorescence stereoscopic photographs of the lungs were taken, the tissues were processed and embedded in OCT compound, and cross sections of 5-μm thickness were prepared for detecting NP distribution by fluorescence photomicroscopy. The tissue specimens were also processed and embedded in paraffin according to standard procedures, and 5-μm sections were cut. Sections were further examined to detect NP distribution by immunostaining.

Direct RV Pressure Measurements

Three weeks after MCT administration, the animals were anesthetized with sodium pentobarbital, and polyethylene catheters were then inserted into the right ventricle through the jugular vein and carotid artery for hemodynamic measurements. RV systolic pressure and systemic blood pressure were measured with a polygraph system (AP-601G, Nihon Kohden).[12,17]

Echocardiographic Measurements of RV and PA Hemodynamics

Transthoracic echocardiographic measurements (Vevo 2100 ultrasound system; Primetech Inc) were performed as described previously.[18] Additional details are provided in the online-only Data Supplement (available at http://hyper.ahajournals.org).

Assessment of Right Heart Hypertrophy and PA Remodeling

After systemic arterial and RV pressures were recorded, the animals were euthanized and the lungs and heart were isolated. The RV wall was dissected from the left ventricle and ventricular septum. Wet weight of the right ventricle and of the left ventricle plus ventricular

septum was determined, and RV hypertrophy was expressed as RV weight/(left ventricle plus ventricular septum weights).[12,17]

The lungs were perfused with a solution of 10% phosphate-buffered formalin (pH 7.4). At the same time, 10% phosphate-buffered formalin (pH 7.4) was administered into the lungs via tracheal tube at a pressure of 20 cm H_2O. These specimens were processed for light microscopy by routine paraffin embedding. The degree of remodeling (muscularization) of small, peripheral, PAs was assessed by double immunohistochemical staining of the 5-μm sections with an anti-α-smooth muscle actin antibody (dilution 1:500; clone 1A4, Dako) and anti-platelet endothelial cell adhesion molecule-1 (PECAM-1) (M-20) antibody (dilution 1:100, Santa Cruz).[12] To assess the type of remodeling of muscular PAs, microscopic images were analyzed. In each rat, 30 to 40 intra-acinar arteries were categorized as muscular (those with a complete medial coat of muscle), partially muscular (those with only a crescent of muscle), or nonmuscular (those with no apparent muscle), counted, and averaged within a range of diameters from 25 to 50 μm.[12]

Histopathologic and Immunohistochemical Analysis of Rat Lungs

The degrees of monocyte infiltration were evaluated by immunostaining for ED-1 (analog of human CD68, Serotec). For quantification, a blinded observer counted the number of ED-1–positive cells in 10 fields. Sections were also subjected to immunostaining with antibodies against FITC (1:1000; American Research Products, Belmont, MA), an epitope (α-p65) on the p65 subunit of NF-κB (1:100; Boehringer Mannheim, Roche Diagnostics, Basel, Switzerland), rabbit eNOS (ABR: PA1–037), murine inducible NOS (iNOS, Transduction Laboratories), or nonimmune mouse IgG (Dako). The α-p65 monoclonal antibody recognizes an epitope on the p65 subunit that is masked by bound inhibitor-κB.[19] Therefore, this antibody exclusively detects activated NF-κB.[19]

Real-Time Quantitative Reverse Transcription–Polymerase Chain Reaction

Real-time polymerase chain reaction amplification was performed with rat cDNA with the use of an ABI PRISM 7000 sequence detection system (Applied Biosystems, Foster City, CA) as described previously.[12,19] TaqMan primers/probes for monocyte chemotactic protein-1, tumor necrosis factor-α, interleukin (IL)-1β, IL-6, intercellular adhesion molecule-1, and glyceraldehyde 3-phosphate dehydrogenase, which served as the endogenous reference, were purchased from Applied Biosystems (Assay-on-Demand gene expression products Rn00580555, Rn99999017, Rn00580432, Rn00561420, and Rn00564227 and TaqMan rodent glyceraldehyde 3-phosphate dehydrogenase control reagents, respectively).

Lipopolysaccharide-Induced Activation of Mouse Monocytes

The mouse macrophage cell line RAW 264.7 was purchased. After bacterial lipopolysaccharide (serotype 0111:B4, Sigma) at 1 μg/mL was added to the cells, each 1.0-mL suspension of pitavastatin at 5 mg/mL, FITC-NP (1 mg/mL PLGA), pitavastatin-NP containing 1.0 mg/mL PLGA and 5 mg/mL pitavastatin, or vehicle was added to the wells; 2 hours later, the cells were washed 3 times with PBS. NF-κB pathway activity was measured with a TransAM NF-κB p65 ELISA-based assay kit (Active Motif, Tokyo, Japan). Nuclear extracts of RAW 264.7 cells were prepared with the NE-PER nuclear and cytoplasmic extraction reagent kit (Pierce, Rockford, IL) according to the manufacture's protocol. Samples were placed, along with 30 μL of binding buffer, on a 96-well plate to which oligonucleotides containing an NF-κB consensus binding site had been immobilized for 1 hour on a shaker. During this time, the activated NF-κB contained in the sample specifically binds to this nucleotide; then the plate was washed and, by using a primary antibody (100 mL diluted 1:1000 in antibody binding buffer for 1 hour) that is directed against the NF-κB p65 subunit, the NF-κB complex bound to the oligonucleotides can be detected. The plate was then washed again, and 100 μL of secondary antibody (diluted 1:1000 in antibody binding buffer) conjugated to horseradish peroxidase was added for 1 hour. The plate was washed again, and 100 μL of developing solution was added. The plate was incubated for 4 minutes away from direct light, 100 μL of stop solution was added, and the plate was read with a plate reader at 450 nm.

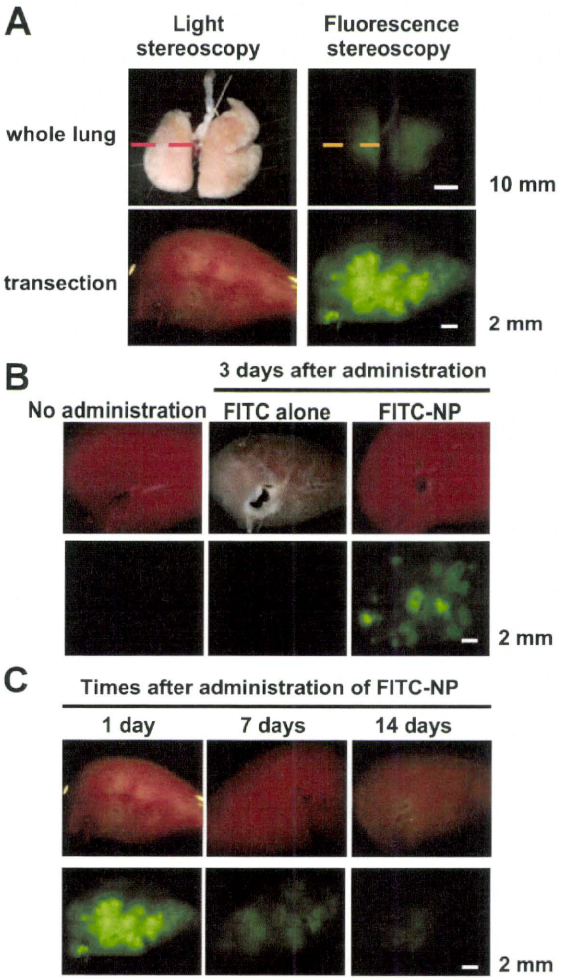

Figure 1. Localization of FITC-NP after instillation into the rat lung. A, Representative light (left) and fluorescence (right) stereomicrographs of whole lungs (upper) and transections (lower) 1 hour after intratracheal instillation of FITC-NP. B, Representative light (upper) and fluorescence (lower) stereomicrographs of transections from control (nontreated) lungs and from lungs instillated with FITC alone or FITC NP on day 3 after instillation. C, Representative light (upper) and fluorescence (lower) stereomicrographs of cross sections from lungs instillated with FITC-NP on days 1, 7, and 14 after instillation.

Western Blot Analysis

Protein was extracted from frozen lung tissues. Samples were homogenized in lysis buffer containing 10 mmol/L Tris-HCl, pH 7.4, 50 mmol/L NaCl, 5 mmol/L EDTA, 1% Triton X-100, 50 mmol/L NaCl, 30 mmol/L sodium phosphate, 50 mmol/L NaF, 1% aprotinin, 0.5% pepstatin A, 2 mmol/L phenylmethylsulfonyl fluoride, and 5 mmol/L leupeptin and phosphatase inhibitor cocktail (Pierce). Cell lysates (50 μg) were separated on 7.5% polyacrylamide gels and blotted onto polyvinylidene difluoride membranes (Millipore Co, Hercules, CA). Protein expression was analyzed by using antibodies against eNOS (ABR: PA1–037) or actin (Sigma). Immune complexes were visualized with horseradish peroxidase–conjugated secondary antibodies. Bound antibodies were detected by chemiluminescence with the use of an ECL detection system (Amersham Biosciences) and quantified by densitometry.

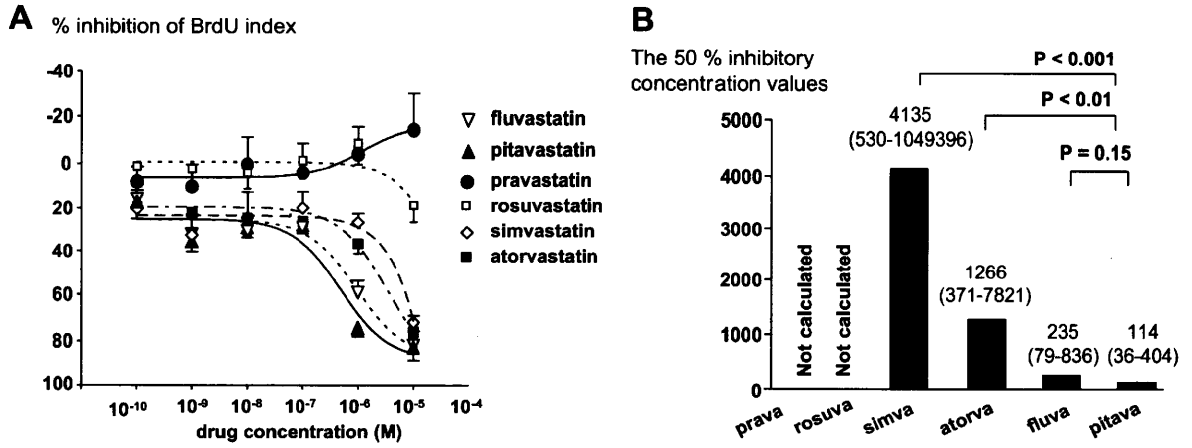

Figure 2. Inhibitory effects of various statins on human PASMC proliferation. A, PASMC proliferation assay (% inhibition of 5′-bromo-2′-deoxyuridine [BrdU] index) in response to various concentrations of various statins (n=6 per group). B, IC_{50} values and 95% Wald CIs (in parentheses) are shown at the top of each bar. Probability values vs pitavastatin by Wald tests in a 4-parameter logistic-regression model are shown. Prava indicates pravastatin; rosuva, rosuvastatin; simva, simvastatin; atorva, atorvastatin; fluva, fluvastatin; and pitava, pitavastatin.

Measurements of Pitavastatin Concentration

Pitavastatin concentrations in serum and lung were measured at predetermined time points by using a column-switching high-performance liquid chromatography system, as previously reported.[20] In brief, the column-switching high-performance liquid chromatography system consists of 2 LC-10AD pumps, an SIL-10A autosampler, a CTO-10A column oven, a 6-port column-switching valve, and an SPD-10A UV detector (all from Shimadzu, Kyoto, Japan). The column temperature was maintained at 40°C. Preprepared serum or tissue homogenate sample solutions were injected from the autosampler into the high-performance liquid chromatography system, and detection of the statin in sample solutions was performed at 250 nm with a UV detector. The detected peak area was measured with Lcsolution software (Shimadzu).

Statistical Analysis

Data are presented as mean±SEM. Statistical analysis of differences was performed by 1-way ANOVA and Bonferroni's multiple comparison tests. The survival rates were determined by the Kaplan-Meier method. Efficacy ratios (median inhibitory concentration [IC_{50}]values) of statins were tested with Wald tests in a 4-parameter logistic-regression model. Point estimates and Wald 95% CIs for IC_{50} values were calculated. Statistical calculations were performed with SAS preclinical package software version 9.1.3 (SAS Institute Inc, Tokyo, Japan) and Prism Software version 4.0.1 (GrafPad). A value of $P<0.05$ was considered statistically significant.

Results

Localization of FITC-NP in the Lung of Rats With MCT-Induced PAH

Localization of FITC was examined after a single intratracheal instillation of FITC-NP into animals injected with MCT. Three days after instillation, strong FITC signals were detected only in FITC-NP–instillated lungs, whereas no or only faint FITC signals were observed in control noninjected lungs and in lungs injected with FITC only (Figure 1). On days 1, 7, and 14, FITC signals remained localized predominantly in the lungs. There were FITC-positive cells in the bronchi and alveoli, alveolar macrophages, and small arteries. As we previously reported,[12] immunofluorescence staining revealed that FITC signals localized mainly in small arteries and arterioles as well as in small bronchi and alveoli 14 days after instillation of FITC-NP (online-only Figure I). FITC signals were not detected in remote organs (liver, spleen, and heart) at any time point (data not shown).

Inhibitory Effects of Statins on Human PASMC Proliferation

To implicate pitavastatin as a candidate statin for nanoparticulation, the effects of statins on PASMC proliferation were examined. In a human PASMC proliferation assay (percent inhibition of 5′-bromo-2′-deoxyuridine index), hydrophilic statins (rosuvastatin and pravastatin) elicited no inhibitory effects, whereas other statins showed dose-dependent effects (Figure 2A). The IC_{50} value of pitavastatin was lower than that of simvastatin or atorvastatin (Figure 2B). The IC_{50} value of pitavastatin tended to be lower than that of fluvastatin, but there was no significant difference in the IC_{50} values between the 2 statins.

Effects of Pitavastatin-NP on the Development of PAH in the Rat Model of MCT-Induced PAH

An RV catheterization study confirmed that injection of MCT led to severe PAH (increased RV systolic pressure) associated with small PA remodeling and increased infiltration of ED1-positive monocytes 3 weeks after MCT injection, as previously reported.[12,17] Single intratracheal treatment with pitavastatin-NP, but not with pitavastatin alone or FITC-NP, attenuated the development of PAH, small PA remodeling, and monocyte-mediated inflammation (Figure 3). The RV systolic pressure of untreated normal controls (no MCT injection) was 34±2 mm Hg (n=10). There were no significant differences in concentrations of pitavastatin in the lung and systemic blood between pitavastatin-NP–treated and pitavastatin-only groups (the Table).

Echocardiographic study showed that there were no significant changes in cardiac output or stroke volume among untreated control and MCT-induced PAH rats (online-only Table I). Echo-derived estimation of RV systolic pressure and pulmonary vascular resistance showed the development of MCT-induced PAH and therapeutic effects of a single intra-

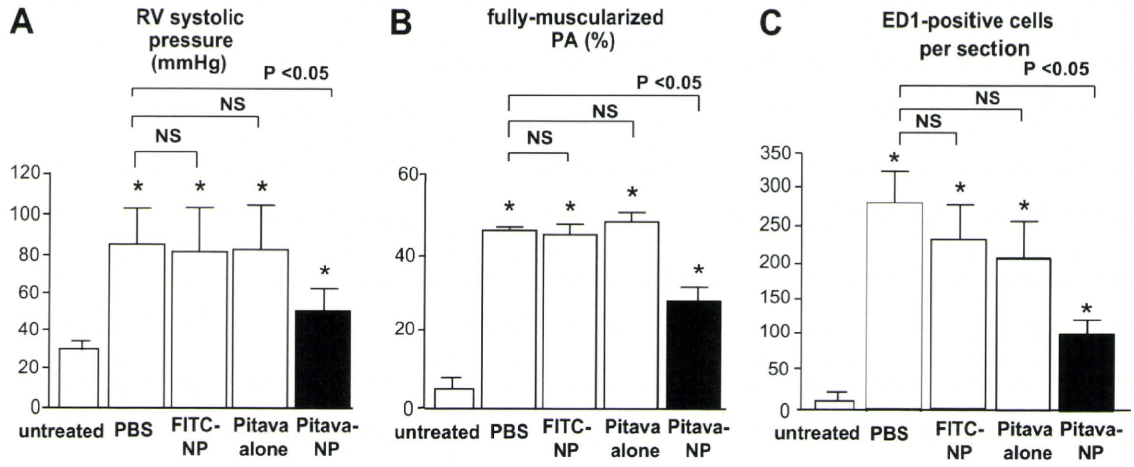

Figure 3. Effects of pitavastatin (pitava)-NP on RV systolic pressure, small PA remodeling, and infiltration of monocytes 3 weeks after MCT injection. A, RV systolic pressure in the 4 experimental groups. Data are mean±SEM (n=6 per group). B, Percentage of fully muscularized small PAs in the 4 experimental groups. Data are mean±SEM (n=6 per group). C, Infiltration of ED1-positive monocytes into the lung (the number of positive cells per 30 high-power-field cross sections). Data are mean±SEM (n=6 per group). *$P<0.01$ vs untreated control.

tracheal instillation of pitavastatin-NP, as reported by the RV catheterization study.

The activity of lactate dehydrogenase was not detected in bronchoalveolar lavage fluid. There were no significant changes in activity of lactate dehydrogenase and various biomarkers in lung tissue homogenates among untreated control and MCT-induced PAH rats (online-only Tables II and III).

Oral daily administration of pitavastatin at 0.3 mg/kg had no significant effects on MCT-induced PAH, but pitavastatin at 1.0, 3.0, and 10 mg/kg significantly attenuated the development of PAH (online-only Figure II).

Effects of Intratracheal Instillation of Pitavastatin-NP on NF-κB Activation and PAMSC Proliferation

As previously reported,[12] immunohistochemically detectable NF-κB activation was noted mainly in alveolar macrophages and weakly in PA lesions 7 days after MCT administration (Figure 4). A single intratracheal instillation of pitavastatin-NP, but not of FITC-NP or pitavastatin alone, markedly attenuated the increases in NF-κB (α-p65) activity induced by MCT injection (Figure 4). Because NF-κB was activated in alveolar monocytes in MCT-induced PAH, effects of pitavastatin-NP on NF-κB activity were examined in a monocyte cell line (RAW 264.7 cells) in vitro. Treatment with pitavastatin-NP, but not with pitavastatin only, attenuated NF-κB activation in RAW 264.7 cells (online-only Figure III). Because proliferation of PASMCs is increased in animals and humans with PAH, effects of pitavastatin and pitavastatin-NP were examined in human PASMCs in vitro. Treatment with pitavastatin-NP, but not with pitavastatin only, attenuated the proliferation of PASMCs (online-only Figure IV).

Table. Pitavastatin Concentrations in the Lung and Systemic Blood After Intratracheal Administration of Pitavastatin (100 μg per Animal) Only or Pitavastatin-NP Containing the Same Dose of Pitavastatin

	Time After Administration, h					
Groups	1	3	6	12	24	48
Pitavastatin-only group						
Lung, ng/g	115±83	49±69	7±5	2±1	3±3	4±3
Serum, ng/mL	48±19	24±10	9±7	1±1	1±1	1±1
Pitavastatin-NP group						
Lung, ng/g	155±77	17±8	13±13	4±6	7±4	3±1
Serum, ng/mL	65±19	20±5	7±4	2±1	1±1	1±2

Data are mean±SEM (n=6 per group).

Effects of Pitavastatin-NP on Expression of Proinflammatory Factors

As previously reported,[12] MCT-induced PAH was associated with increased gene expression of proinflammatory factors. Intratracheal treatment with pitavastatin-NP significantly reduced the increased gene expression of monocyte chemotactic protein-1, tumor necrosis factor-α, and IL-6 and tended to decrease the expression of IL-1β and intercellular adhesion molecule-1 (online-only Figure V).

Effects of Pitavastatin-NP on eNOS and iNOS Expression

Because the protective effects of statins on PAH have been reported to be attributable at least to the eNOS-related pathway,[11] eNOS protein expression in the lungs was examined on days 3 and 21 after treatment. Western blot analysis showed that MCT administration had no significant effect on eNOS expression on days 3 and 21, compared with untreated controls (Figure 5). Pitavastatin-NP, but not FITC-NP or pitavastatin alone, increased the protein expression of eNOS on day 3, whereas pitavastatin-NP showed no therapeutic effects on eNOS expression on day 21 (Figure 5).

In contrast, iNOS is known to cause oxidant tissue injury and accelerates the pathologic processes of PAH.[21] Immuno-

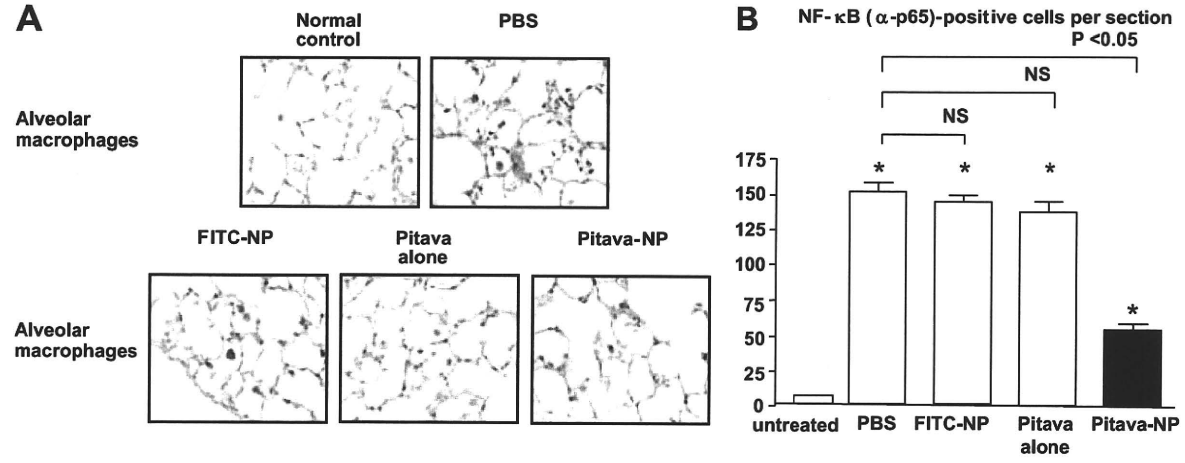

Figure 4. Effects of pitavastatin (pitava)-NP on NF-κB activation. A, Photomicrographs of cross sections of lung stained immunohistochemically with NF-κB (α-p65) from normal rats and PAH rats 3 days after MCT injection. B, Effects of pitavastatin-NP on infiltration of NF-κB (α-p65)–positive cells 3 days after MCT injection. Data are mean±SEM (n=6 per group). *$P<0.01$ vs untreated control.

histochemical expression of iNOS was not detected in lung sections from untreated control rats. Immunostaining for iNOS was noted mainly in alveolar macrophage and weakly in PA lesions 3 days after MCT administration (online-only Figure VI). Single intratracheal instillation of pitavastatin-NP, but not of FITC-NP or pitavastatin only, markedly attenuated the increase in iNOS activity induced by MCT injection.

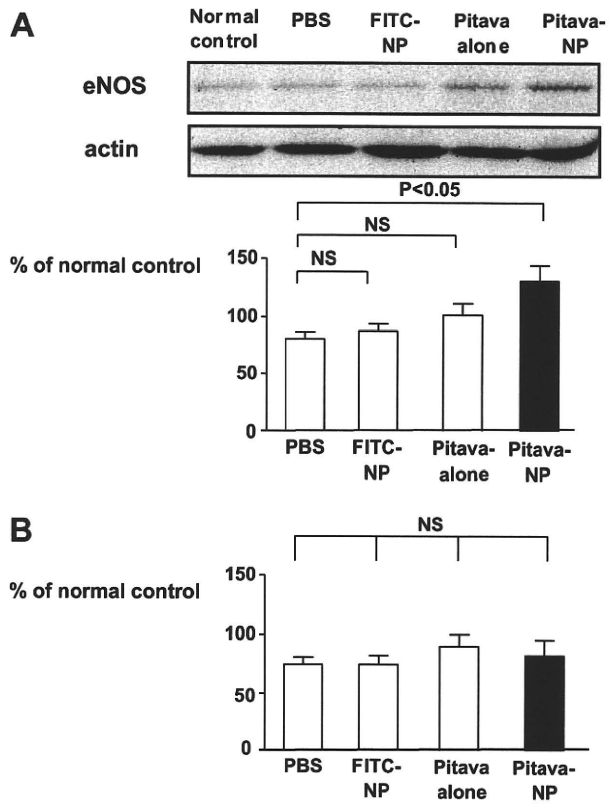

Figure 5. Effects of pitavastatin (pitava)-NP on eNOS protein expression. A, eNOS expression in the lung 3 days after MCT injection. The eNOS level is shown as a percentage of the internal-control actin level. n=6 per group. B, eNOS expression in the lung 21 days after MCT injection. The eNOS level is shown as a percentage of the internal-control actin level. n=6 per group.

Effects of Pitavastatin-NP on Survival

In the treatment protocol, pitavastatin-NP significantly improved survival rate: 42% in the PBS group (n=40), 39% in the FITC-NP group (n=33), 40% in the pitavastatin-alone group (n=40), and 64% in the pitavastatin-NP group (n=58; Figure 6). In addition, pitavastatin-NP caused regression of MCT-induced PAH (Figure 6).

Discussion

We recently reported that intratracheal instillation of a polyethylene glycol-*block*-PLGA copolymer (PEG-PLGA) is an excellent system for drug delivery to the lung.[12] We found in the present study that PLGA NPs were as effective as PEG-PLGA NPs as an NP-mediated drug delivery system to the lung. As we reported with PEG-PLGA NPs,[12] the FITC signals were detected in small bronchial tracts, alveolar macrophages, and small PAs for up to 14 days after a single instillation of FITC-encapsulated PLGA NP.

Statins are known to ameliorate the effects of endothelial injury/dysfunction by enhancing the activity of eNOS and thus, exert multiple vasculoprotective effects on other cell types (vascular smooth muscle cells, monocytes, etc).[3–5] We recently reported that NP-mediated pitavastatin delivery to the vascular endothelium of ischemic skeletal muscles effectively increased therapeutic neovascularization in a murine model of hindlimb ischemia.[13] In our previous study, the beneficial effects of pitavastatin-NP were mediated by increased activity of eNOS.[13] Notably, NP-mediated delivery of pitavastatin had greater angiogenic activity in human endothelial cells in vitro compared with pitavastatin alone.[13] We therefore hypothesized that eNOS and downstream pathogenetic factors might be involved in the therapeutic effects of NP-mediated pitavastatin delivery on MCT-induced PAH. Among statins, pitavastatin was selected as the nanoparticulation compound because this drug elicited the most potent angiogenic effects in human endothelial cells[14] and the most

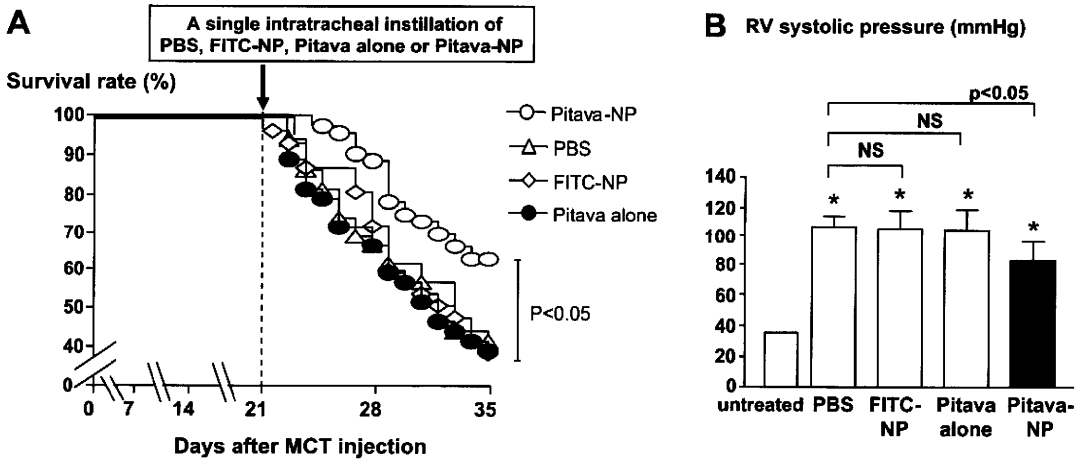

Figure 6. Effects of pitavastatin (pitava)-NP on RV systolic pressure and survival rate. A, Survival curves analyzed by the Kaplan-Meier method in PBS, FITC-NP, pitavastatin only, and pitavastatin-NP groups. B, RV systolic pressure (in mm Hg) in the 4 experimental groups 2 weeks after treatment (at week 5 after MCT injection).

potent inhibitory effects on human PASMC proliferation (Figure 2) in vitro compared with other statins. We also found that NP-mediated intracellular delivery of pitavastatin showed greater inhibitory effects on PASMC proliferation and on NF-κB activation in a monocyte cell line (RAW 264.7 cells) compared with pitavastatin alone (online-only Figures III and IV). Collectively, these in vitro data suggest that NP-mediated pitavastatin delivery is more effective than pitavastatin in inhibiting PASMC proliferation and monocyte activation and improving the deleterious effects of endothelial injury/dysfunction.

The important novel finding of the present study is that a single intratracheal instillation of pitavastatin-NP attenuated the development of PAH (increased RV pressure, PA resistance, and PA remodeling) associated with reduced activity of NF-κB and NF-κB–dependent inflammatory factors (for example, monocyte chemotactic protein-1, IL-1, tumor necrosis factor-α, iNOS, etc). In contrast, eNOS expression was not reduced in the PBS group but was increased by day 3 only but not by day21 (Figure 5), suggesting that eNOS plays a minor role in the therapeutic effects of pitavastatin-NP. Intratracheal instillation of pitavastatin alone at the same dose had no therapeutic effect. Concentrations of pitavastatin in the lungs and systemic blood were found to be similar between animals treated with pitavastatin-NP and those treated with pitavastatin only (the Table). These findings suggest a specific advantage of NP-mediated delivery of pitavastatin to induce therapeutic effects. Therefore, the beneficial effects of pitavastatin-NP on MCT-induced PAH in vivo can be attributable to the pleiotropic effects of pitavastatin-NP, including inhibition of inflammation and cell proliferation.

Prior studies have reported that daily oral administration of statins at high doses beyond the clinical norm (a regimen that could lead to serious adverse side effects in a clinical setting) attenuates MCT- and hypoxia-induced PAH in animals.[7–9] We thus examined whether NP-mediated pitavastatin delivery would be superior to daily oral administration of pitavastatin alone in inhibiting MCT-induced PAH, and we found that oral daily administration of pitavastatin at 0.3 mg/kg per day for 21 days (cumulative dose=25.2 mg per animal, assuming the body weight of animals to be 250 g) had no therapeutic effects, but the same regimen of pitavastatin at 1, 3, and 10 mg/kg per day (cumulative doses=84, 252, and 840 mg per animal, respectively) did show significant therapeutic effects. Therefore, our NP-mediated delivery system (single injection of 0.1 mg pitavastatin per animal) seems to be as effective at an ≈840-times lower dose than the cumulative systemic dose.

It is noteworthy that a single intratracheal treatment with pitavastatin-NP 3 weeks after MCT injection induced regression of PAH and improved survival rate. This finding is more clinically significant than is the mere prevention of PAH. These results suggest that this NP-mediated delivery of pitavastatin may have beneficial therapeutic effects in patients with established PAH.

Perspectives

This mode of NP-mediated delivery of pitavastatin into the lungs is more effective in attenuating the development of MCT-induced PAH compared with intratracheal treatment with pitavastatin alone or systemic administration of pitavastatin, and treatment with pitavastatin-NP induced regression of established PAH. For translation of our present findings into clinical medicine, more clinical studies are needed to investigate whether pitavastatin-NP by inhalation might be effective in improving PAH.

Source of Funding

This study was supported by Health Science Research grants (Research on Nano-medicine and on Intractable Diseases) from the Ministry of Health Labor and Welfare, Tokyo, Japan.

Disclosures

Dr Egashira holds a patent on the results reported in this study. The remaining authors report no conflicts of interest.

References

1. Farber HW, Loscalzo J. Pulmonary arterial hypertension. *N Engl J Med.* 2004;351:1655–1665.
2. Humbert M, Sitbon O, Simonneau G. Treatment of pulmonary arterial hypertension. *N Engl J Med.* 2004;351:1425–1436.

3. Takemoto M, Liao JK. Pleiotropic effects of 3-hydroxy-3-methylglutaryl coenzyme A reductase inhibitors. *Arterioscler Thromb Vasc Biol.* 2001; 21:1712–1719.
4. Egashira K, Hirooka Y, Kai H, Sugimachi M, Suzuki S, Inou T, Takeshita A. Reduction in serum cholesterol with pravastatin improves endothelium-dependent coronary vasomotion in patients with hypercholesterolemia. *Circulation.* 1994;89:2519–2524.
5. Egashira K. Clinical importance of endothelial function in arteriosclerosis and ischemic heart disease. *Circ J.* 2002;66:529–533.
6. Ni W, Egashira K, Kataoka C, Kitamoto S, Koyanagi M, Inoue S, Takeshita A. Anti-inflammatory and antiarteriosclerotic actions of HMG-CoA reductase inhibitors in a rat model of chronic inhibition of nitric oxide synthesis. *Circ Res.* 2001;89:415–421.
7. Girgis RE, Mozammel S, Champion HC, Li D, Peng X, Shimoda L, Tuder RM, Johns RA, Hassoun PM. Regression of chronic hypoxic pulmonary hypertension by simvastatin. *Am J Physiol.* 2007;292: L1105–L1110.
8. Nishimura T, Faul JL, Berry GJ, Vaszar LT, Qiu D, Pearl RG, Kao PN. Simvastatin attenuates smooth muscle neointimal proliferation and pulmonary hypertension in rats. *Am J Respir Crit Care Med.* 2002;166: 1403–1408.
9. Nishimura T, Vaszar LT, Faul JL, Zhao G, Berry GJ, Shi L, Qiu D, Benson G, Pearl RG, Kao PN. Simvastatin rescues rats from fatal pulmonary hypertension by inducing apoptosis of neointimal smooth muscle cells. *Circulation.* 2003;108:1640–1645.
10. McMurtry MS, Bonnet S, Michelakis ED, Bonnet S, Haromy A, Archer SL. Statin therapy, alone or with rapamycin, does not reverse monocrotaline pulmonary arterial hypertension: the rapamycin-atorvastatin-simvastatin study. *Am J Physiol.* 2007;293:L933–L940.
11. Rhodes CJ, Davidson A, Gibbs JS, Wharton J, Wilkins MR. Therapeutic targets in pulmonary arterial hypertension. *Pharmacol Ther.* 2009;121: 69–88.
12. Kimura S, Egashira K, Chen L, Nakano K, Iwata E, Miyagawa M, Tsujimoto H, Hara K, Morishita R, Sueishi K, Tominaga R, Sunagawa K. Nanoparticle-mediated delivery of nuclear factor-κB decoy into lungs ameliorates monocrotaline-induced pulmonary arterial hypertension. *Hypertension.* 2009;53:877–883.
13. Kubo M, Egashira K, Inoue T, Koga J, Oda S, Chen L, Nakano K, Matoba T, Kawashima Y, Hara K, Tsujimoto H, Sueishi K, Tominaga R, Sunagawa K. Therapeutic neovascularization by nanotechnology-mediated cell-selective delivery of pitavastatin into the vascular endothelium. *Arterioscler Thromb Vasc Biol.* 2009;29:796–801.
14. Oda S, Nagahama R, Nakano K, Matoba T, Kubo M, Sunagawa K, Tominaga R, Egashira K. Nanoparticle-mediated endothelial cell-selective delivery of pitavastatin induces functional collateral arteries (therapeutic arteriogenesis) in a rabbit model of chronic hind limb ischemia. *J Vasc Surg.* 2010;52:412–420.
15. Kawashima Y, Yamamoto H, Takeuchi H, Hino T, Niwa T. Properties of a peptide containing DL-lactide/glycolide copolymer nanospheres prepared by novel emulsion solvent diffusion methods. *Eur J Pharm Biopharm.* 1998;45:41–48.
16. Kawashima Y, Yamamoto H, Takeuchi H, Fujioka S, Hino T. Pulmonary delivery of insulin with nebulized DL-lactide/glycolide copolymer (PLGA) nanospheres to prolong hypoglycemic effect. *J Control Release.* 1999;62:279–287.
17. Ikeda Y, Yonemitsu Y, Kataoka C, Kitamoto S, Yamaoka T, Nishida K, Takeshita A, Egashira K, Sueishi K. Anti-monocyte chemoattractant protein-1 gene therapy attenuates pulmonary hypertension in rats. *Am J Physiol Heart Circ Physiol.* 2002;283:H2021–H2028.
18. Urboniene D, Haber I, Fang YH, Thenappan T, Archer SL. Validation of high-resolution echocardiography and magnetic resonance imaging versus high-fidelity catheterization in experimental pulmonary hypertension. *A J Physiol.* 2010;299:401–412.
19. Ohtani K, Egashira K, Nakano K, Zhao G, Funakoshi K, Ihara Y, Kimura S, Tominaga R, Morishita R, Sunagawa K. Stent-based local delivery of nuclear factor-κB decoy attenuates in-stent restenosis in hypercholesterolemic rabbits. *Circulation.* 2006;114:2773–2779.
20. Kojima J, Fujino H, Yosimura M, Morikawa H, Kimata H. Simultaneous determination of NK-104 and its lactone in biological samples by column-switching high-performance liquid chromatography with ultraviolet detection. *J Chromatogr.* 1999;724:173–180.
21. Hampl V, Bibova J, Banasova A, Uhlik J, Mikova D, Hnilickova O, Lachmanova V, Herget J. Pulmonary vascular iNOS induction participates in the onset of chronic hypoxic pulmonary hypertension. *Am J Physiol.* 2006;290:L11–L20.

ONLINE SUPPLEMENT

Nanoparticle-Mediated Delivery of Pitavastatin into Lungs Ameliorates Development and Induces Regression of Monocrotaline-induced Pulmonary Arterial Hypertension

Ling Chen, Kaku Nakano, Satoshi Kimura, Tetsuya Matoba, Eiko Iwata, Miho Miyagawa, Hiroyuki Tsujimoto, Kazuhiro Nagaoka, Junji Kishimoto, Kenji Sunagawa, Kensuke Egashira

Department of Cardiovascular Medicine (LC, KN, TM, EI, MM, KN, KS, KE) and Digital Medicine Initiative (JK), Graduate School of Medical Science, Kyushu University, Fukuoka, Japan; and Hosokawa Micron Corporation (HT), Osaka, Japan.

Address for correspondence:

Kensuke Egashira, M.D. Ph.D.
Department of Cardiovascular Medicine
Graduate School of Medical Science, Kyushu University
3-1-1, Maidashi, Higashi-ku,
Fukuoka 812-8582, Japan
Phone : +81-92-642-5358
Fax : +81-92-642-5375
E-mail: egashira@cardiol.med.kyushu-u.ac.jp

Materials and Methods

Echocardiographic measurements of RV and PA hemodynamics

Transthoracic 2-D, M-mode and pulsed-wave Doppler Echo were obtained with a 30 MHz transducer (Vevo 2100 ultrasound system; Primetech Inc). [1] M-mode and 2-D modalities were applied to measure RV free wall thickness during end diastole and RV wall stress. These images were obtained from the right side of the rat, with the ultrasonic beam positioned perpendicularly to the wall of the midthird of the RV.

PA diameter was measured at the level of pulmonary outflow tract during midsystole using the superior angulation of the parasternal short-axis view. M-mode measurements were performed from "leading edge to leading edge" (epicardial to endocardial) as recommended by the American Society of Echocardiography.

Pulsed-wave Doppler was used to measure PA acceleration time (PAAT) and PA flow velocity time integral. The Doppler sample volume was centrally positioned within the main PA, just distal from the pulmonary valve with the beam oriented parallel to the flow. The sweep speed for the Doppler flow recordings was 400–800 mm/s. RV ejection time was measured as the interval from the onset to the end of ejection in milliseconds. Thereafter, pulmonary artery acceleration time normalized for cycle length, RV systolic pressure, and pulmonary vascular resistance (PVR) were estimated. Stroke volume (SV), CO, and cardiac index (CI) were also calculated.

Measurement of lactate dehydrogenase To examine cytotoxicity of intratracheal treatment of pitavastatin-NP, the activity of lactate dehydrogenase (LDH) in bronchoalveolar lavage fluid (BALF) and lung tissue homogenates was measured 7 days after MCT administration using an assay kit LDH (Wako Pure Chemical Industries, Ltd.) according to the manufacturer's instructions in separate series of experiments.

Measurement of biomarkers by multiplex immunoassay Tissue concentrations of various biomarkers in ling tissue homogenates were measured 7 days after MCT administration using the Luminex LabMAP instruments (Table III), which was ordered to biomarker analysis services of Charles River Inc (http://www.criver.com/en-US/ProdServ/ByType/Discovery/Pages/PlasmaBiomarkerAnalysis.aspx).

1. Urboniene D, Haber I, Fang YH, Thenappan T, Archer SL. Validation of High-Resolution Echocardiography and Magnetic Resonance Imaging Versus High-Fidelity Catheterization in Experimental Pulmonary Hypertension. *Am J Physiol Lung Cell Mol Physiol.*

Table S1. Echocardiographic characteristics of untreated control and MCT-induced PAH rats in prevention study

parameters	untreated control	MCT-induced PAH			
		PBS	FITC NP	Pitava alone	Pitava-NP
Cardiac output (mL/min)	120 ± 17	97 ±21	104 ±20	102 ±20	113 ±16
Stroke volume (mL)	0.29±0.04	0.24±0.05	0.26±0.06	0.26±0.05	0.28±0.05
Heart rate (beats per minute)	412 ± 26	408 ±36	399 ±39	397 ±32	405 ±25
PAAT/cl (x 100)	18 ±1	7 ±1*	7 ±1*	7 ±1*	12 ±1*†
eRVSP (mmHg)	20 ±3	65 ±11*	66 ±9*	62 ±7*	41 ±5 *†
PVR (mmHg/ml/min)	0.12 ±0.02	0.46 ±0.20*	0.43 ±0.12*	0.40 ±0.01*	0.24 ±0.05*†
RV wall thickness (mm)	0.64 ±0.05*	1.16 ±0.14*	1.05 ±0.10*	0.97 ± 0.06*	0.88 ±0.09*†
RV wall stress	20 ±5	48 ±19*	56 ± 26*	48 ±12*	24 ±8†

Data are the mean± SEM (n=6 each).
*P< 0.05 versus untreated control group
† P< 0.05 versus PBS group.
Abbreviations: PAAT/cl = normalized pulmonary artery acceleration time; eRVSP = estimated RV systolic pressure; PVR = pulmonary vascular resistance.

Table S2. Lactate dehydrogenase activity in cell-free bronchial lavage fluid and lung tissue homogenates 7 days after monocrotaline administration

Sample sites	Untreated control	monocrotaline			
		PBS group	FITC NP group	Pitava alone group	Pitava NP group
bronchial lavage fluid (IU/mL)	ND	ND	ND	ND	ND
Lung tissue (IU/ng protein)	8.6±3.4	2.8±1.1	10.9±6.0	5.7±4.6	11.8±4.9

Data are the mean± SEM (n=6 each). ND = not detected (under limit of detection).
There is no significant difference (P=0.56) among 5 groups by one-way ANOVA.

Table S3. Cytokines and other proteins in lung tissue homogenates 7 days after monocrotaline administration

parameters	unit	Untreated control	PBS group	FITC NP group	Pitava alone group	Pitava NP group
Apo A1	μg/mg	0.14±0.05	0.10±0.03	0.09±0.01	0.10±0.01	0.10±0.01
CD40	pg/mg	N.D.	N.D.	N.D.	N.D.	N.D.
CD40 Ligand	pg/mg	43±16	34±14	25±3	30±8	39±13
CRP	μg/mg	1.3±0.3	1.2±0.2	1.3±0.4	1.3±0.2	1.6±0.2
ET-1	pg/mg	61±36	67±29	61±18	64±15	56±15
Eotaxin	pg/mg	49±12	53±15	40±8	45±17	63±11
EGF mouse	pg/mg	0.54±0.21	0.55±0.21	0.40±0.08	0.44±0.09	0.44±0.07
Factor VII	ng/mg	0.53±0.12	0.58±0.17	0.47±0.07	0.48±0.07	0.53±0.08
FGF-9	ng/mg	0.10±0.02	0.09±0.03	0.07±0.01	0.08±0.01	0.08±0.03
FGF-basic	ng/mg	0.21±0.04	0.21±0.06	0.17±0.04	0.22±0.04	0.24±0.04
GCP-2 Rat	pg/mg	6.5±1.6	7.4±3.2	6.7±1.3	8.1±1.0	7.6±7
GM-CSF	pg/mg	N.D.	N.D.	N.D.	N.D.	N.D.
Haptoglobin	μg/mg	0.80±0.30	1.13±0.40	1.04±0.26	1.19±0.12	1.18±0.25
IFN-gamma	pg/mg	0.12±0.06	0.24±0.09	0.23±0.10	0.18±0.07	0.18±0.05
IP-10	pg/mg	1.7±0.3	2.2±1.0	1.7±0.3	1.7±0.5	2.1±0.8
IL-1 alpha	pg/mg	5.3±4.8	9.7±7.1	4.6±1.0	7.8±2.9	5.7±3.3
IL-1 beta	ng/mg	N.D.	N.D.	N.D.	N.D.	N.D.
IL-10	pg/mg	3.1±1.5	2.5±1.5	1.4±0.8	1.8±0.3	1.9±0.9
IL-11	pg/mg	9.8±5.6	6.1±1.6	6..1±4.8	5.9±1.0	6.8±2.0
IL-12p70	pg/mg	1.5±0.4	1.3±0.4	1.2±0.4	1.0±0.1	1.2±0.4
IL-17A	pg/mg	0.2±0.04	0.2±0.09	0.2±0.05	0.2±0.05	0.2±0.02
IL-18	ng/mg	0.2±0.1	0.2±0.1	0.2±0.1	0.2±0.0	0.2±0.1
IL-2	pg/mg	1.7±0.7	1.4±1.1	0.6±0.3	0.8±0.6	0.9±0.7
IL-3	pg/mg	1.1±0.5	0.9±0.3	0.9±0.4	0.7±0.3	0.8±0.2
IL-4	pg/mg	N.D.	N.D.	N.D.	N.D.	N.D.
IL-5	ng/mg	N.D.	N.D.	N.D.	N.D.	N.D.
IL-6	pg/mg	N.D.	N.D.	N.D.	N.D.	N.D.
IL-7	pg/mg	3.9±0.7	3.5±2.0	3.4±0.8	3.0±0.3	3.2±0.6
LIF	pg/mg	33.9±9.8	38.3±12.5	29.9±4.3	31.6±4.1	35.7±6.1
Lymphotactin	pg/mg	1.7±0.4	2.0±0.7	1.8±0.3	1.6±0.1	1.78±0.4
MIP-1alpha	ng/mg	0.05±0.02	0.06±0.02	0.05±0.01	0.05±0.00	0.05±0.01
MIP-1beta	pg/mg	26.7±7.6	36.8±13.2	30.9±13.2	27.1±5.2	28.2±5.8
MIP-2	pg/mg	1.7±1.0	1.3±0.3	1.5±0.5	1.8±0.9	1.8±0.5
MIP-3 beta	ng/mg	0.1±0.0	0.2±0.1	0.1±0.0	0.2±0.0	0.2±0.0
MDC	pg/mg	14±5	11±3	12±1	15±5	15±3
MMP-9	pg/mg	16±3	13±6	13±3	14±3	13±3
MCP-1	pg/mg	14±2	17±4	17±4	16±4	20±4
MCP-3	pg/mg	12±3	14±4	13±3	13±3	16±4
MPO	ng/mg	26±12	25±14	15±4	15±5	26±6
Myoglobin	ng/mg	109±26	157±130	138±67	135±54	133±69
OSM	pg/mg	9±2	11±3	9±1	9±0.001	10±2
SAP	pg/mg	0.007±0.002	0.007±0.002	0.006±0.001	0.008±0.001	0.008±0.001
SGOT	μg/mg	N.D.	N.D.	N.D.	N.D.	N.D.
SCF	pg/mg	920±509	404±71	421±143	603±440	531±110
RANTES	pg/mg	0.82±0.51	0.55±0.35	0.56±0.50	0.56±0.31	0.56±0.25
TPO	ng/mg	0.41±0.09	0.39±0.15	0.32±0.11	0.23±0.14	0.27±0.08
TF	ng/mg	0.15±0.03	0.15±0.05	0.15±0.03	0.14±0.03	0.14±0.04

TIMP-1	pg/mg	4±8	3.8±1.2	3.6±0.8	3.5±0.5	3.6±0.6
TNF-alpha	ng/mg	2.4±0.5	2.7±0.7	2.3±0.5	2.1±0.2	2.2±0.5
VCAM-1	ng/mg	4.8±1.0	5.4±1.8	5.2±1.0	5.2±0.9	5.8±0.7
VEGF-A	pg/mg	749±297	759±281	924±317	791±181	689±214
vWF	ng/mg	0.6±0.2	0.5±0.2	0.4±0.1	0.5±0.1	0.5±0.1

Data are mean ± SEM (n= 6 each).

Multiplex immunoassay were peformed using the Luminex LabMAP instruments.

Apo A1 (Apolipoprotein A1), CD (cluster of differentiation), CRP (C Reactive Protein), EGF (Epidermal Growth Factor), FGF-9 (Fibroblast Growth Factor-9), FGF-basic (Fibroblast Growth Factor-basic), GCP-2 (Granulocyte Chemotactic Protein-2), GM-CSF (Granulocyte Macrophage-Colony Stimulating Factor), GST-a (Glutathione S-Transferase alpha), IFN-g (Interferon-gamma), IgA (Immunoglobulin A), IL (Interleukin), IP-10 (Inducible Protein-10), LIF (Leukemia Inhibitory Factor), MCP (Monocyte Chemoattractant Protein), MDC (Macrophage-Derived Chemokine), MIP (Macrophage Inflammatory Protein), MMP-9 (Matrix Metalloproteinase-9), MPO (Myeloperoxidase), OSM (Oncostatin M), RANTES (Regulation Upon Activation, Normal T-Cell Expressed and Secreted), SAP (Serum Amyloid P), SCF (Stem Cell Factor), SGOT (Serum Glutamic-Oxaloacetic Transaminase), TIMP-1 (Tissue Inhibitor of Metalloproteinase Type-1), TNF-a (Tumor Necrosis Factor-alpha), TPO (Thrombopoietin), VCAM-1 (Vascular Cell Adhesion Molecule-1), VEGF (Vascular Endothelial Cell Growth Factor), vWF (von Willebrand Factor). N.D. (Not Detected).

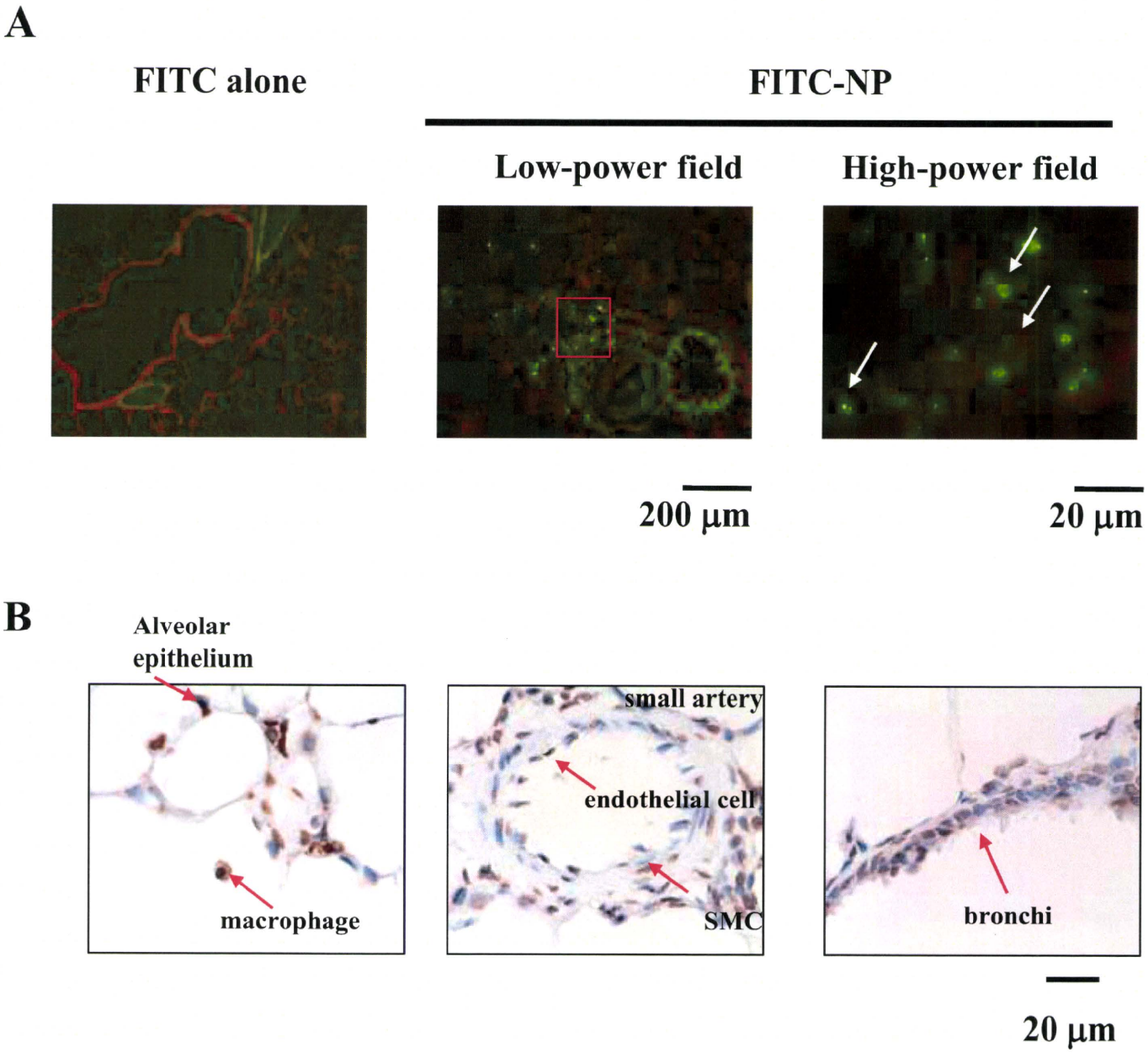

Figure S1. Localization of FITC alone and FITC-NP post-instillation in the rat lung. A, Fluorescent micrographs of cross-sections from lung instillated with FITC alone and FITC-labeled NP on day 3 post-instillation. Nuclei were counterstained with propidium iodide (red). Scale bars: 200 μm and 20 μm.
B, Micrographs of cross-sections stained immunohistochemically against FITC from lung instillated intratracheally with FITC-NP on days 14 post-instillation.

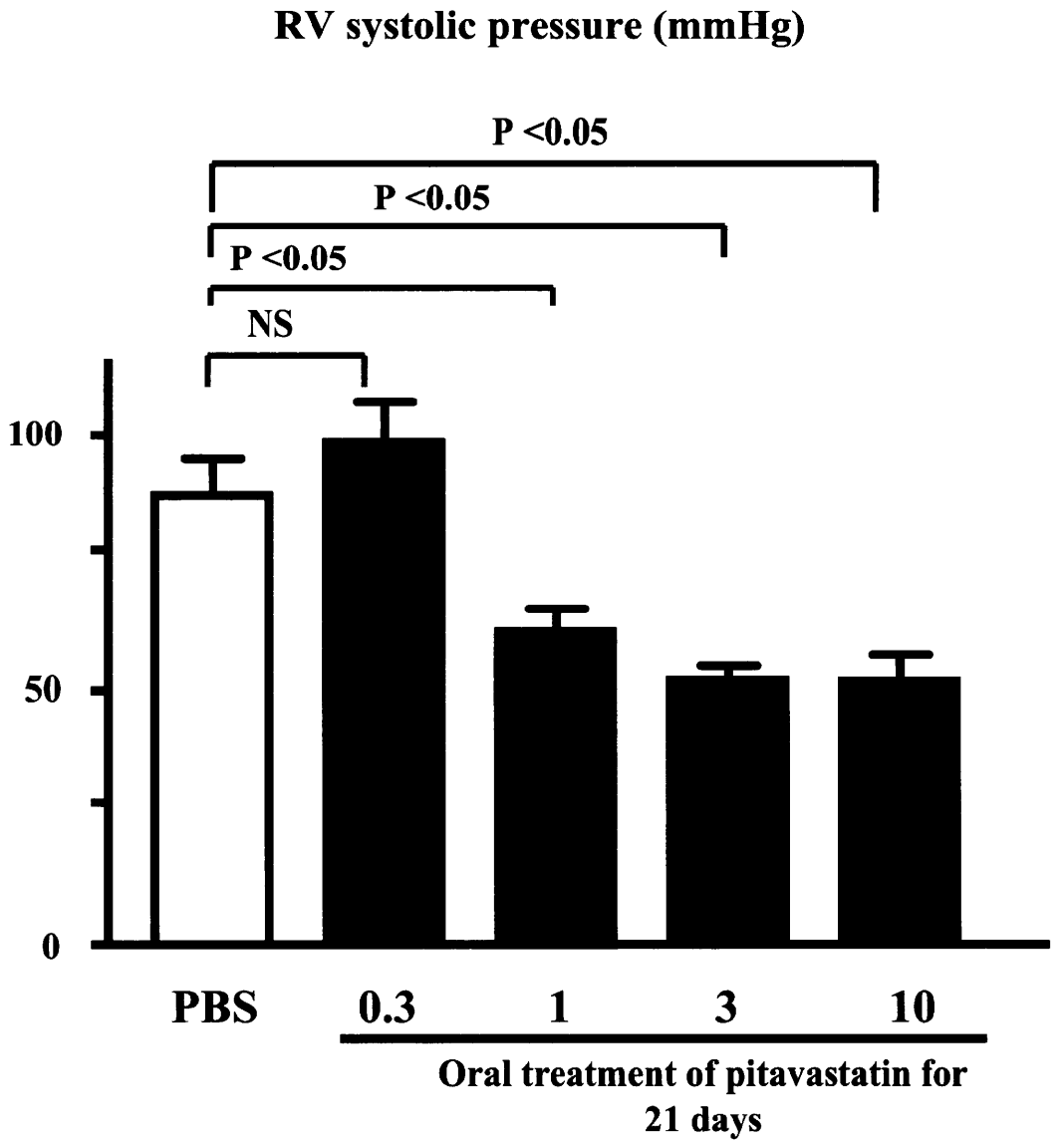

Figure S2. Effects of oral treatment of pitavastatin on right ventricular (RV) systolic pressure 3 weeks after MCT injection. Data are mean ± SEM ($n = 6$ each).

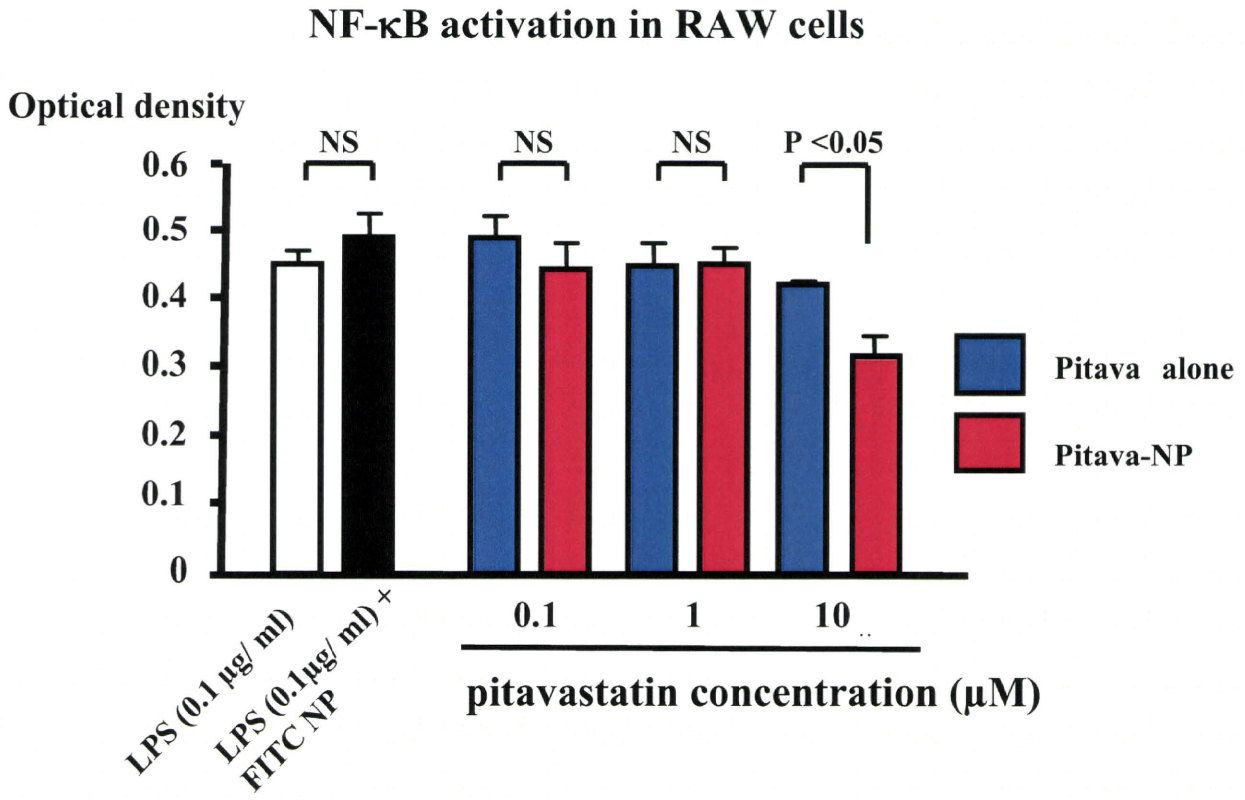

Figure S3 Effect of pitavastatin-NP on NF-κB activation of monocyte cell line (RAW cells)
Effects of pitavastatin-NP on LPS-stimulated activation of NF−κB (ELISA-based DNA binding assay against NF-kB p65 subunit: arbitrary unit). Data are mean ± SEM (n= 6 each).

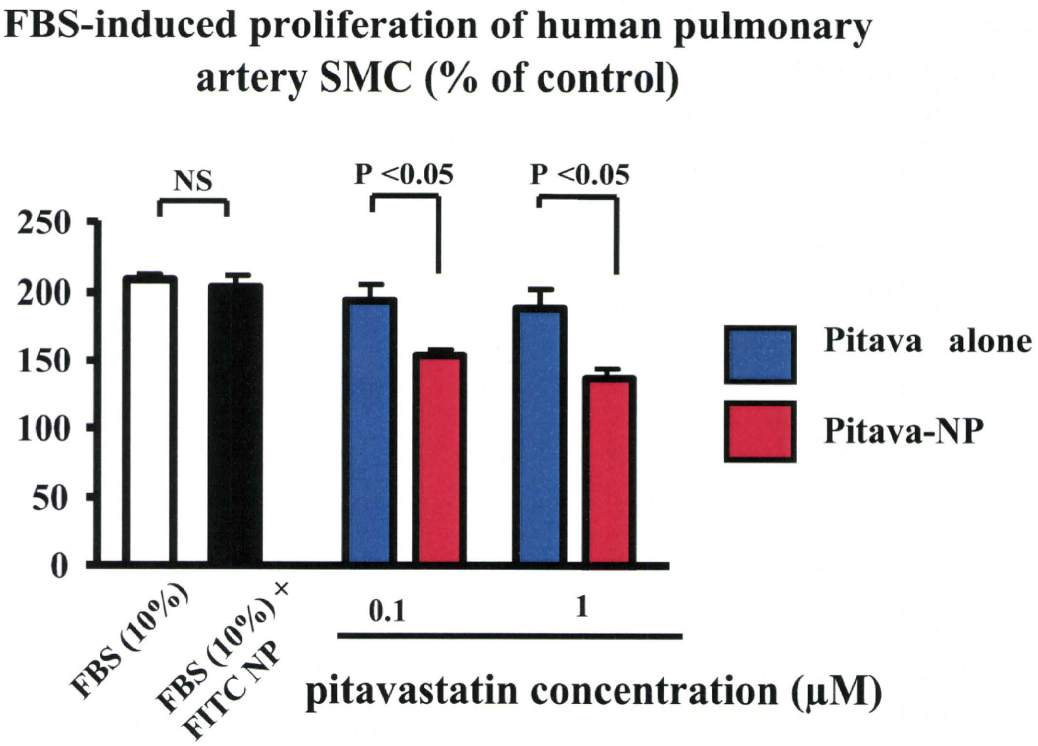

Figure S4. Effects of pitavastatin-NP versus pitavastatin on FBS-induced proliferation of human PASMCs (cell count per well). Data are mean ± SEM (n = 6 each).